Journal Name

COMMUNICATION

Hierarchically Porous MOF/polymer Composites via Interfacial Nanoassembly and Emulsion Polymerization

Received 00th January 20xx,
Accepted 00th January 20xx

DOI: 10.1039/x0xx00000x

www.rsc.org/

Peng Jin, [a] Wenlong Tan,[a] Jia Huo,*[a,b] Tingting Liu, [a] Yu Liang,[a] Shuangyin Wang,*[a] and Darren Bradshaw* [c]

In this work, we develop a general strategy for the preparation of robust hierarchically porous and readily processable MOF composites through an interfacial nanoassembly/emulsion polymerization method. MOF nanoparticles of different composition and stability including ZIF-8, UiO-66 and Cr-MIL-101 and moisture-sensitive HKUST-1 have been successfully incorporated into the composites. The size of macropores within the ZIF-8/polystyrene (ZIF-8/PS) composites can be controlled from 6 µm to 28.5 µm through changing the amount of MOF nanoparticles, which simultaneously tunes the loading of MOFs within the composites. The fluidic nature of the emulsion before polymerization facilitates the processibility of the MOF-composites into task-specific shapes, including columns, spheres, and various irregular bodies. Additionally, the magnetic functionality can be endowed to the MOF composites through co-assembly of Fe_3O_4 and MOF nanoparticles. The MOF composites exhibit excellent mechanical stability even after pressing or long-term mechanical stirring, and the ZIF-8/PS polyHIPE shows high conversion rate toward the Knoevenagel reaction compared with bulk ZIF-8 nano- and microparticles.

Metal-organic frameworks (MOFs) are assembled by metal ions or clusters with organic ligands through coordination interactions to form organic-inorganic hybrid porous materials.[1-3] Because of their highly ordered pore structure, high internal surface areas, and chemical functionality, MOFs have been attracting strong research interest and can be widely used in various fields, such as gas separation,[4-5] pollutant removal,[6] sensing,[7-8] drug delivery,[9-10] fuel cells and energy storage,[11-12] and catalysis.[13-17] For MOFs to be of practical use in these applications however, a degree of processing beyond the as-made bulk powders is often desirable,[18] and shape-engineering[19] of MOFs is a key driver to enhance their application-specific properties and handling. The shaping of MOFs into monolithic and other structures is particularly important,[20-23] and ideally the resulting structured materials will display hierarchical porosity for high mass diffusion, be easy to handle and physically robust, and the combination of MOFs with easily processable organic polymers provides a convenient strategy to address these criteria.[24-29]

PolyHIPEs are porous emulsion-templated polymers derived from high internal phase emulsions (HIPEs) that can be used to prepare high surface area beads, monoliths and membranes for wide-ranging applications.[30] Macroporous polyHIPEs have previously been used as scaffolds for MOF growth to prepare hierarchically porous MOF/polymer composite monoliths[31] and beads[32] with readily tuneable MOF contents and increased (MOF) mechanical stability. More recently, Majaz et al have reported hydrostable MOF-polyHIPEs through transformation of immobilized metal oxide particles[33] and a report by Shirshova and co-workers[34] details a simultaneous crystallisation-polymerisation process to generate MOF-polyHIPE materials in a single step without the need to pre-form the polyHIPE, but in this final case the recorded MOF loadings were comparatively low.

PolyHIPES can also be prepared from emulsions that are stabilised by nanoparticles of diverse composition to access functional macroporous composites[35-38]. This relies on the Pickering-stabilisation of the HIPE emulsion template, and we (and others) have previously demonstrated that a number of prototypical MOFs have suitable surface wettability and colloidal stability for the effective stabilisation of both oil-in-water and reverse phase emulsions.[13, 39, 40] We have exploited this property for the emulsion-templating of MOF/polymer composite capsules for pH-triggered release of encapsulated dye molecules[41], and the preparation of magnetic-MOF composite capsules for the encapsulation of large functional biomolecules for recyclable size-selective biocatalysis[13].

In this contribution, we extend this work to develop an interfacial nanoassembly and emulsion polymerization

[a] State Key Laboratory of Chem/Bio-Sensing and Chemometrics, Provincial Hunan Key Laboratory for Graphene Materials and Devices, College of Chemistry and Chemical Engineering, Hunan University, Changsha, 410082, Hunan, China. E-mail: jiahuo@hnu.edu.cn; shuangyinwang@hnu.edu.cn
[b] Shenzhen Research Institute of Hunan University, Shenzhen 518057, Guangdong, China.
[c] School of Chemistry, University of Southampton, Highfield Campus, Southampton SO17 1BJ, UK. E-mail: D.Bradshaw@soton.ac.uk

† Electronic Supplementary Information (ESI) available: See DOI: 10.1039/x0xx00000x

strategy where the continuous rather than the dispersed phase[41] of a MOF-stabilized Pickering emulsion[42] is polymerized to prepare robust hierarchically porous MOF-polyHIPE phases. (Figure 1a) This strategy should permit controlled localisation of the MOF within the emulsion-templated macropores, allow MOF contents to be readily adjusted and facilitate shaping due to the fluid nature of the MOF-stabilized HIPE[27]. It is also expected to be applicable to a wide range of MOFs as the process is largely governed by the surface properties of the framework particles which are readily tuneable.

ZIF-8 is a tetrahedrally-connected framework constructed from zinc(II) ions and 2-methylimidazole that displays high thermal and chemical stability,[43, 44] and has previously been employed to provide Pickering-stabilisation to emulsion droplets[41]; hence, ZIF-8 was taken as an exemplar material for validating the concept of interfacial nanoassembly and emulsion polymerisation for the preparation of hierarchically porous MOF-polyHIPE composites. ZIF-8/PS composites were fabricated by employing a water-in-oil (w/o) emulsion polymerization technique based on high internal phase emulsions (HIPEs)[45] containing the MOF nanoparticles in water as the dispersed phase and mixtures of polymeric monomers (styrene and divinylbenzene (DVB)) and the swelling agent (oleic acid) as the continuous phase (see experimental section for full details). After shearing, polymerization, and washing, bulk ZIF-8/PS monolithic composites were obtained (Figure 1b-d).

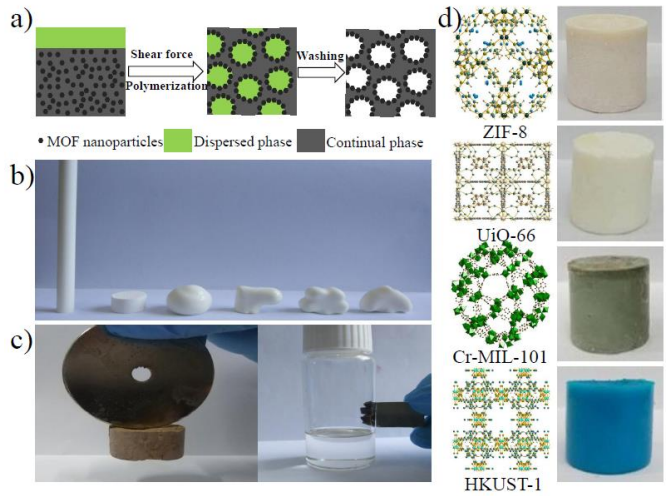

Figure 1. a) Illustration of the interfacial assembly/polymerization fabrication procedure for the preparation of hierarchically porous MOF/polymer composites; b) Various shapes of hierarchically porous ZIF-8/PS by casting the emulsion into moulds prior to polymerization; c) Magnetic functionalization and recovery of ZIF-8/PS containing < 2 wt% magnetite; d) Representative MOF/polymer composites obtained using this strategy.

The ZIF-8/PS composites were cut into small pieces for characterization of the interior surface by scanning electron microscopy (SEM) as shown in Figure 2. SEM images of ZIF-8/PS (Figure 2b-d) show the as-prepared materials possess a foam-like structure containing well-separated macroporous cavities with an average diameter of 17 µm. The size of the resulting macropores is comparable to that of the emulsion droplets before polymerization (Figure S1), indicating the ZIF-8 stabilized Pickering emulsions acted as direct templates for macropore formation. We note that ZIF-8 nanoparticles are homogeneously distributed over the internal surface of each of the macropores in an approximate monolayer, and since the nanoparticles were pre-assembled at the w/o interface during the polymerization process,[46-48] this strategy permits localisation of the ZIF-8 component in a controlled manner within the composite polyHIPE. This arrangement would be beneficial for the access of guests during catalysis or separation applications, and no change in ZIF-8 nanoparticle shape or size (~ 120 nm) is observed after the polymerization process (Figure 2d). The structure of the ZIF-8/PS composite was further characterized by powder X-ray diffraction (PXRD). As shown in Figure 2e, a series of diffraction peaks at 2θ = 7.3, 10.3, 12.7, 14.7, 16.4, 18.0° are observed that match well with those of as-prepared and simulated ZIF-8,[44, 49] and no other impurity is present except for the broad peak at ~ 2θ = 20° resulting from the amorphous PS component. The PXRD data thus confirm the ZIF-8 nanoparticles incorporated within the polyHIPE composites retain their original sodalite structure.[44]

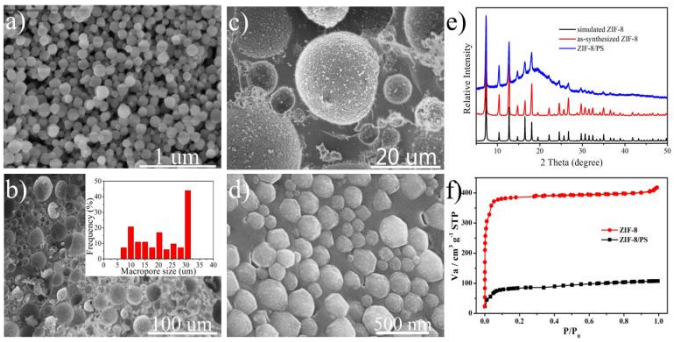

Figure 2. Low (a-b) and high magnification (c-d) SEM images of ZIF-8 nanoparticles (a) and cross-section of ZIF-8/PS composites (b-d) (inset of (b) is the macropore size distribution of ZIF-8/PS evaluated from the size of macropores in SEM images).(e) PXRD patterns of simulated ZIF-8, the ZIF-8 nanoparticles used for emulsion stabilisation, and the ZIF-8/PS composite; and (f) N_2 sorption/desorption isotherms of ZIF-8 nanoparticles and the ZIF-8/PS composite.

The microporosity of ZIF-8/PS was revealed by the N_2 adsorption/desorption isotherm shown in Figure 2f. Although the specific surface area (BET method) of ZIF-8/PS is reduced from 1610 $m^2 g^{-1}$ for bulk ZIF-8 nanoparticles to 299 $m^2 g^{-1}$, the ZIF-8/PS composite largely displays a type I isotherm and a pore size predominantly in the microporous range consistent with the presence of the ZIF-8 nanoparticles (Figure S2) used to stabilise the emulsion. Mesopores with an average diameter of 38 nm are also observed, likely resulting from the continual phase, which should further ensure efficient guest permeation between the ZIF-8 lined macropores (Figure S2).

To clarify the origin of the mesoporosity and the contribution of the PS component to the overall specific surface area, ZIF-8 nanoparticles were fully removed by soaking the ZIF-8/PS composites in acetic acid solution (Figure S3). The specific surface area of the resultant PS-only architecture decreases to 11 $m^2 g^{-1}$ (Figure S4), confirming that

the N_2 adsorption capacity of the composite largely arises from the incorporation of the ZIF-8 nanoparticles. Further, the pore size distribution following ZIF-8 removal confirms that the mesoporous contribution to the overall (pore-size) distribution of the composite originates from the polymer continual phase (Figure S4). The reduction of the specific surface area for ZIF-8/PS is thus reasonable considering it is mixed with an amorphous macroporous polymer.

Thermogravimetric analysis (TGA) shows the amount of ZIF-8 nanoparticles within the ZIF-8/PS composite is 18.6 wt% (Figure S5), which is in good agreement with inductively coupled plasma optical emission spectrometry (ICP-OES) following composite calcination and oxide digestion (Table S4). The composite surface area is fully consistent with that expected for this loading level. The sorption data of ZIF-8/PS thus demonstrate that the micropores of ZIF-8 in the composites remain open to guest access, which is corroborated by SEM images revealing the particles are only partially embedded in the polymer (continual) phase. This clearly results from the appropriate surface wettability of the ZIF-8 particles which partition effectively to the w/o interface during Pickering stabilisation[41], a property that has also been exploited to prepare ZIF-8/67 Janus-type particles using a polymer mask[50].

The connectivity between the macropores is important for practical applications in areas dependent on mass transport, since it directly determines the ability of analytes or substrates to penetrate into the polymer foams.[51, 52] To investigate the influence of swelling agents on the pore structure, different molecules were employed as swelling agents during the synthesis of the ZIF-8/PS composites including heptane, dodecane, liquid paraffin, and oleic acid, as well as a control sample without any swelling agent (i.e. monomers only) present. The microporosity of the ZIF-8/PS composites prepared with different swelling agents is revealed by the N_2 adsorption/desorption isotherms shown in Figure S6 (and data Table S1). Mesopores with different sizes are also observed, and the corresponding pore-size distributions show that ZIF-8/PS prepared with oleic acid has the largest mesopore size.

Oil red was chosen as a probe molecule to reveal the ability of the guest to penetrate into the hierarchically porous ZIF-8/PS composites. The as-prepared composite foams were cut into small pieces (0.5 × 0.4 × 0.4 cm^3) and soaked in an oil red solution in toluene for 6 h, and then cross-sectioned to evaluate the extent of guest penetration into the composite interior. Unquestionably, the sample prepared without any swelling agent appears almost nonporous prohibiting the diffusion of the oil red into the cross-linked polystyrene as evidenced by the almost white interior of the composite after soaking in the dye solution (Figure S7), which is consistent with the reduction in surface area and mesoporosity of the composite in the absence of oleic acid (Figure S2c, S6). Oil red could penetrate into the polymer matrices for all of the other samples prepared in the presence of swelling agents, but the composite prepared in the presence of oleic acid revealed the best guest penetration ability forming a homogeneously deep red colour throughout the interior (Figure S7a). This phenomena is reasonable in view of the differences of the solubility parameter and structure between the swelling agents and polystyrene matrices.[41]

The solubility parameters (δ) of the swelling agents used differ sharply with that of the polystyrene (Figure S7b), promoting efficient phase separation and thus resulting in the formation of pores for guest diffusion within cross-linked polymers consistent with our previous reports.[41] Interestingly, although oleic acid has a similar solubility parameter with the polystyrene, it contains both hydrophilic and hydrophobic groups at each end, and may act as a surfactant so that numbers of oleic acid could gather to form reverse micelles in non-aqueous monomer solution,[51, 53] which could potentially create the observed mesopores and thus improve the penetration ability of the oil red within the ZIF-8/PS composite. Although our investigation of swelling agents has initially focussed on neutral molecules, a range of ionic species such as CTAB may also be employed which may offer additional emulsion stabilisation and permit further control and tuneability of the porosity within the composites (Figure S6).

As described, the macropores present in the composite monoliths are the inverse replica of the ZIF-8-Pickering-stabilized emulsions, hence the size of the macropores can be readily modified by tuning the diameter of the emulsion droplets. Figure S9-S13 clearly show that by increasing the amount of ZIF-8 nanoparticles from 0.3 g to 3.0 g, the average macropore size decreases from 28.5 μm to 6 μm (inset of Figure S8 and Table S2) and the pore size distribution becomes gradually more narrow. Concomitantly, the proportion of ZIF-8 within the composites increases from 7.2 to 40.7 wt% as determined from TGA data (Figure S14 and Table S3), which is at similar levels to the deposition of MOFs into pre-formed macroporous polyHIPE matrices.[31, 32] The tuneable macropore diameter mainly arises from the increased nanoparticle content which prompts the decrease of the size of dispersed droplets for the arrangement of ZIF-8 nanoparticle monolayers during the formation of Pickering-stabilized emulsions.[54]

Many industrial applications require the processing of MOFs into task-specific configurations, including membranes, capsules, pellets and monoliths.[55] Since the MOF-stabilized emulsions prepared here are in a fluid state before polymerization, the resulting composites could be easily configured into different entities using shaped moulds as reactors where the polymerization happens[56], as previously described by Wang and co-workers for magnetic MOF-based composite foams[27]. This concept was validated through filling various vials/moulds with emulsions followed by polymerization, as shown by the photographic images in Figure 1b and 1d. It shows that the final morphologies adopted by the composites take on the shape of the reactor with no significant shrinkage following drying (Figure S15). Composite morphology can thus be easily varied, and we have successfully prepared columnar composites of varying aspect ratio, spheres, and irregular bodies, which could find special application; for example, MOF-polymer monolithic composite columns can be used for chromatography.[57-59]

As the requirement for interfacial nanoassembly is dependent on the surface properties (e.g. surface wettability, zeta-potential) of the emulsion stabilising nanoparticles rather than their absolute composition *per se*, we can further functionalize the MOF composites.[41] For example, magnetic recyclability is easily achieved through mixing a small amount of Fe_3O_4 nanoparticles with the ZIF-8, without the need to preform magnetic core/shell MOF nanoparticle materials.[27] As shown in Figure 1c, incorporation of < 2wt% Fe_3O_4 in the ZIF-8/PS composite endows the as-prepared materials with strong permanent magnetic properties permitting easy separation from a reaction solution. EDX elemental mapping of Fe reveals that the Fe_3O_4 is uniformly distributed throughout the composite, although there are a few small clusters that appear to coincide with the location of macropores. (Figure S16 and Figure S17) Physical robustness is a prerequisite for practical application of materials, determining their durability under actual operating conditions.[60] The hierarchically porous ZIF-8/PS is physically robust and no significant deformation of the composite is observed even after application of modest force using a 1.5 kg weight (Figure 3a). Physical stability was also evaluated through mechanical stirring: the composites were stirred in water or toluene at 400 rpm for 12 h, and fully retained their morphology and structural integrity (Figure 3b and Figure S18).

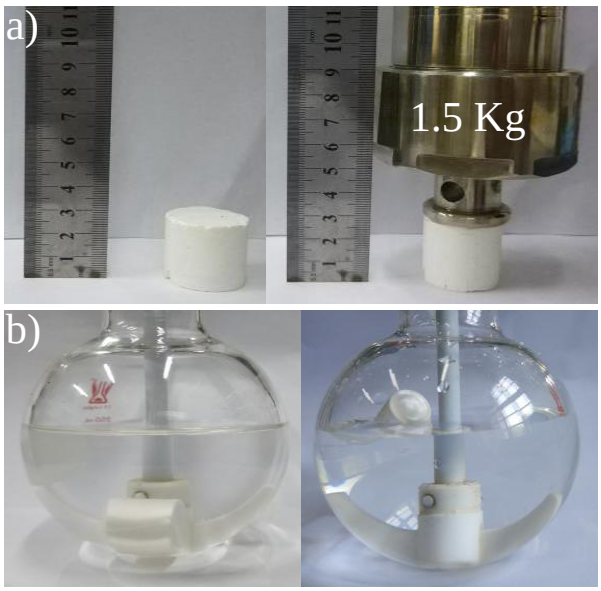

Figure 3. (a) Pressing experiment of the ZIF-8/PS before (left) and after (right) conducted with a 1.5 kg autoclave; and (b) Mechanical stability test of the ZIF-8/PS stirred in the toluene (left) or water (right) for 12 h .

We further investigated the generality of our interfacial nanoassembly and emulsion polymerisation strategy by extending to two other MOF types. The first type are moisture-stable MOFs (*cf*. ZIF-8) including UiO-66[61] and MIL-101-Cr[62] with different compositions and topologies (Figure S19), and the second type is moisture-sensitive HKUST-1.[63] The synthetic procedure for UiO-66 is similar to the ZIF-8 system with styrene and DVB used as polymerizable monomers, whereas for MIL-101-Cr a small amount of 4-vinylpyridine was added as a co-monomer in the presence of NaCl to enhance the MOF-polymer interface and emulsion stability, respectively, consistent with our previous report.[41] PXRD patterns clearly reveal that UiO-66 and MIL-101-Cr have been successfully incorporated into the composites (Figure S20) without disrupting their structures. SEM images in Figure S21 show that UiO-66 and MIL-101-Cr behave in an identical way to ZIF-8 nanoparticles to form hierarchically porous MOF/PS composites with well-separated macropores whose internal surfaces were closely packed with the MOF nanoparticles which retain their original size (~ 216 nm and ~ 442 nm, respectively) and shape. The loading levels of UiO-66 and MIL-101-Cr within their corresponding composites are 8.1 and 12.9 wt%, respectively, determined from TGA data (Figure S22). The macropore size distribution is relatively narrow and the average macropore sizes for the UiO-66 and MIL-101-Cr systems are 14 and 25 μm, respectively. UiO-66/PS and MIL-101-Cr/PS exhibit typical type I isotherms (Figure S23-S24) as expected, and the specific surface areas of the UiO-66/PS and MIL-101-Cr/PS composites decreased from 1086 and 2212 m^2 g^{-1} for the bulk UiO-66 and MIL-101-Cr nanoparticles to 84 and 289 m^2 g^{-1}, respectively, which is fully consistent with the MOF contents derived from TGA.

For moisture-sensitive HKUST-1 it is not possible to use the previously outlined protocol to synthesize hierarchically porous MOF composites due to framework degradation in aqueous solution.[64] Therefore, inverse o/w emulsions were employed to prepare HKUST-1 composites, where HKUST-1 pre-dispersed in liquid paraffin acted as a dispersive phase and an aqueous solution containing acrylamide, N,N'-methylene-bisacrylamide, and N-isopropylacrylamide as the continuous phase (the as-obtained materials are labelled as HKUST-1/PAM). The introduction of N-isopropylacrylamide is important since the as-prepared polymer is temperature-responsive, which would result in phase separation at temperatures above 32°C to potentially improve the permeability within the final composite.[41] SEM images of HKUST-1/PAM are shown in Figure 4, which indicate macroporous composites with an average pore size of 29 μm have been prepared. The nanoparticles are still packed throughout the internal surface of the macropores and their shape and size (~ 230 nm) are unchanged after polymerization. Furthermore, all diffraction peaks in the PXRD pattern of HKUST-1/PAM can be assigned to that of the original HKUST-1 nanoparticles, confirming that the o/w emulsion polymerization process did not destroy the crystal structure of these moisture-sensitive HKUST-1 nanoparticles. These results indicate that reverse-phase emulsions are equally effective for the preparation of MOF-polymer composites via Pickering-stabilised poly-HIPEs, and provides a means to include potentially moisture sensitive frameworks.

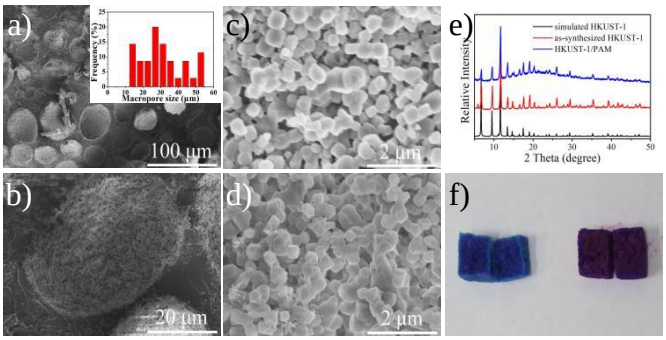

Figure 4. SEM images of the cross-section of hierarchically porous HKUST-1/PAM polyHIPE composites (a-c) and pristine HKUST-1 nanoparticles (average size 230 nm) before the interfacial assembly (d) (inset of (a) is the macropore size distribution within HKUST-1/PAM); (e) PXRD patterns of simulated HKUST-1, HKUST-1 nanoparticles, and HKUST-1/PAM; and (f) Photos of split pieces of HKUST-1/PAM before (left) and after (right) soaking in a Rhodamine B solution.

HKUST-1/PAM also exhibits a typical type I isotherm, confirming the presence of micropores within the composites (Figure S25a). The specific surface area of the HKUST-1/PAM composite is 136 m^2 g^{-1} (bulk HKUST-1 = 1089 m^2 g^{-1}) in excellent agreement with the loading of HKUST-1 from TGA data (the weight percentage of HKUST-1 is 12.3 wt%, Figure S26) and ICP-OES (Table S4). Mesopores with an average diameter of 3.5 nm are also observed, most likely resulting from the continual phase constructed with the cross-linked polyacrylamides, which would ensure guest permeation between macropores (Figure S25b). The porosity and PXRD data are indicative of the structural integrity of HKUST-1 even after polymerization of the emulsion. This is because the framework may not directly contact the aqueous solution during the polymerization, since these nanoparticles were dispersed in the hydrophobic solvent, preventing the diffusion of water into the interior of HKUST-1 which could degrade the frameworks. A similar strategy is often employed to restrict functionalisation to the external surface of MOF particles, where a solvent incompatible with the functional group transformation occupying the porous network prevents the reaction occurring throughout the crystal interior.[65]

Rhodamine B was used as a probe to detect the permeability of the hierarchically porous HKUST-1/PAM composites by soaking in an ethanolic Rhodamine B solution for 2 h. The colour of the interior changed from blue to violet throughout confirming the guest could diffuse freely within the macroporous composites (Figure 4f). The results mentioned above confirm our interfacial nanoassembly and polymerization process is a general strategy to synthesize hierarchically porous MOF/polymer composites, regardless of their composition, topologies, and stability toward moisture.

Hierarchically porous emulsion-templated MOFs[66] and post-synthetically metallated polymer foams[40,67,68] have previously been investigated for their catalytic activity which is generally enhanced using these fabrication strategies either through their increased porosity or the ready incorporation of functional nanoparticles. The robust hierarchically porous ZIF-8/PS composite prepared here was thus tested as a heterogeneous catalyst using the Knoevenagel condensation reaction between malononitrile and benzaldehyde[69] (Figure 5a). For comparison, the catalytic properties of ZIF-8 nanoparticles (~120 nm) and microparticles (~150 μm) were also evaluated. The curves of % conversion versus reaction time for the composite and particulate catalysts are shown in Figure 5b. ZIF-8/PS clearly shows the best catalytic performance among the samples tested, achieving 86.5 and 99.8% conversion into benzylidene malononitrile after 2 and 6 h, respectively (Figure 5b and Figure S29). Control experiments with macroporous PS following acid removal of the ZIF-8 nanoparticles do not exhibit any catalytic activity thus behaving as the blank reaction (no catalyst), confirming that the observed catalytic enhancement derives from the ZIF-8 and not the polymer matrix (Figure 5b). The conversion and yield of the Knoevenagel condensation catalysed by ZIF-8/PS is much higher than those catalysed by ZIF-8 microparticles (32.5 and 60.0 % conversion rates after 2 and 6 h, respectively), and since the PS component is largely inactive this confirms the decrease in size of ZIF-8 leads to the improvement of catalytic activity, since the reaction mainly occurs on the surface of catalysts by consideration of the small window size of the ZIF-8 framework.[69]

More interestingly, the catalytic activity of ZIF-8/PS is even superior to that of ZIF-8 nanoparticles (45.1 and 76.6% conversion after 2 and 6 h, respectively). The increased activity observed for the composite clearly indicates that the macroporous polyHIPE network does not limit mass diffusion[20] and that substrates and products can enter and leave the composite in an unhindered fashion. To understand the reason for this increased activity, we measured the benzaldehyde adsorption properties of ZIF-8/PS and porous PS without ZIF-8 (Figure S30). After soaking these materials in a toluene solution containing benzaldehyde for 6 h, the concentration of benzaldehyde in the solution declined by around 8 percent. This suggests that the concentration of reactants may accumulate within the macropores of the composites to increase the reaction rate, facilitated by the nature and structure of the PS matrix and the favourable localization of the active ZIF-8 within those pores. We also should keep in mind that the ZIF-8 nanoparticles are partially embedded within the polymer matrices which may act to prevent particle aggregation during the reaction[70, 71], which could also lead to an increase in the conversion rate compared with ZIF-8 nanoparticles only.

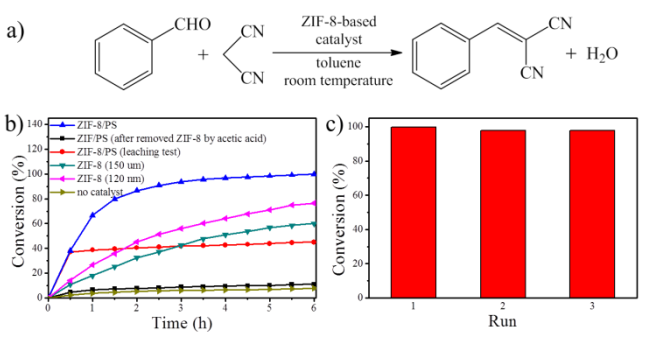

Figure 5. a) Knoevenagel condensation reaction of malononitrile with benzaldehyde catalyzed by ZIF-8-based catalysts; b) Conversion vs. time profiles for the reaction in (a) using ZIF-8 nanoparticles, ZIF-8 microparticles, and ZIF-8/PS composite catalysts, and the leaching test for ZIF-8/PS; and c) Catalytic recycling performance of the ZIF-8/PS composite.

After the reaction, the catalysts could be easily reused following filtration and reactivation because of the bulk characteristics of the composites. These results also demonstrate that the hierarchically porous ZIF-8/PS exhibits not only the high catalytic activity even higher than that of ZIF-8 nanoparticles but also the recyclability of bulk materials. The leach test shows that no reaction happened after the ZIF-8/PS composites were removed from the reaction solution, indicating the catalysts are quite stable without decomposition during the reaction. The heterogeneous nature of the ZIF-8/PS facilitates the recovery of the composite catalyst and no obvious loss of the conversion rate is observed after reusing the ZIF-8/PS composite for at least three cycles (Figure 5c).

In summary, we have demonstrated a general and convenient method to synthesize hierarchically porous MOF/polymer composites through an interfacial nanoassembly and emulsion-polymerization strategy by employing a polyHIPE template Pickering-stabilized by MOF nanoparticles to achieve simultaneously the formation of porosity across multiple length scales and easy MOF processibility. The size of macropores within the HIPE template can be controlled by changing the amount of MOF nanoparticles, and the MOF composites can be readily shaped into spheres, columns, and irregular particles by casting the MOF-stabilized emulsion into moulds prior to polymerization. Owing to the advantageous surface wettability of MOF nanoparticles, this method can be generalized to different MOF systems, including ZIF-8, UiO-66, and MIL-101, and moisture-sensitive HKUST-1. The MOF composites can be easily magnetically functionalized through co-assembly of Fe_3O_4 and MOF nanoparticles.

The hierarchically porous MOF/polymer composites exhibit robust mechanical properties, and no shape change or deformation was observed on application of pressure or mechanical stirring, which is crucial for practical applications. The merit of hierarchically porous MOF composites was evidenced by the catalytic performance of the Knoevenagel condensation catalysed by ZIF-8/PS composites, in which the composite shows better conversion rate than ZIF-8 micro- and nanoparticles which we attribute to the accumulation effect of hierarchically porous PS matrices, unhindered substrate diffusion, and the ordered arrangement of ZIF-8 nanoparticles localized within the macropores of the composite. The high versatility and simultaneous achievement of hierarchical porosity and processibility using this new approach, together with the robust mechanical property and magnetic functionality could further advance the potential of MOFs and their composites in practical applications such as catalysis and separation.

Conflicts of interest

There are no conflicts to declare.

Acknowledgements

The authors acknowledge support from the National Natural Science Foundation of China (Grant No.: 51503062 and 21573063), the Provincial Natural Science Foundation of Hunan (Grant No.: 2017JJ3025), Shenzhen Science and Technology Innovation Committee (Grant No.: JCYJ20170306141630229), and the Fundamental Research Funds for the Central Universities.

Notes and references

1. H. Furukawa, K. E. Cordova, M. O'Keeffe and O. M. Yaghi, *Science*, 2013, **341**, 1230444.
2. R. Kumar, D. Raut, I. Ahmad, U. Ramamurty, T. K. Maji and C. N. R. Rao, *Mater. Horiz.*, 2014, **1**, 513-517.
3. E. Gkaniatsou, C. Sicard, R. Ricoux, J. P. Mahy, N. Steunou and C. Serre, *Mater. Horiz.*, 2017, **4**, 55-63.
4. Q. Xu, D. H. Liu, Q. Y. Yang, C. L. Zhong and J. G. Mi, *J. Mater. Chem.*, 2010, **20**, 706-714.
5. S. Qiu, M. Xue and G. Zhu, *Chem Soc Rev* 2014, **43**, 6116-6140.
6. M. J. Katz, J. E. Mondloch, R. K. Totten, J. K. Park, S. T. Nguyen, O. K. Farha and J. T. Hupp, *Angew. Chem. Int. Ed.*, 2014, **53**, 497-501.
7. F. Y. Yi, Y. Wang, J. P. Li, D. Wu, Y. Q. Lan and Z. M. Sun, *Mater. Horiz.*, 2015, **2**, 245-251.
8. M.-X. Wu and Y.-W. Yang, *Adv. Mater.,* 2017, **29**, 1606134.
9. J. Della Rocca, D. Liu and W. Lin, *Acc. Chem. Res.*, 2011, **44**, 957-968.
10. M. Gimenez-Marques, T. Hidalgo, C. Serre and P. Horcajada, *Coord. Chem. Rev.*, 2016, **307**, 342-360.
11. M. Jahan, Z. Liu and K. P. Loh, *Adv. Funct. Mater.*, 2013, **23**, 5363-5372.
12. L. Wang, Y. Han, X. Feng, J. Zhou, P. Qi and B. Wang, *Coord. Chem. Rev.*, 2016, **307**, 361-381.
13. A. Corma, H. García and F. X. Llabrés i Xamena, *Chem. Rev.*, 2010, **110**, 4606-4655.
14. J. Huo, J. Aguilera-Sigalat, S. El-Hankari and D. Bradshaw, *Chem. Sci.*, 2015, **6**, 1938-1943.
15. X. Li, Q. Jiang, S. Dou, L. Deng, J. Huo and S. Wang, *J. Mater. Chem. A*, 2016, **4**, 15836-15840.
16. X. Wang, X. Li, C. Ouyang, Z. Li, S. Dou, Z. Ma, L. Tao, J. Huo and S. Wang, *J. Mater. Chem. A*, 2016, **4**, 9370-9374.
17. S. Feng, X. Y. Li, J. Huo, Q. L. Li, C. Xie, T. T. Liu, Z. G. Liu, Z. J. Wu and S. Y. Wang, *Chemcatchem*, 2018, **10**, 796-803.
18. D. Bradshaw, A. Garai and J. Huo, *Chem. Soc. Rev.*, 2012, **41**, 2344-2381.
19. B. Valizadeh, T. N. Nguyen and K. C. Stylianou, *Polyhedron*, 2018, **145**, 1-15.
20. E. V. Ramos-Fernandez, M. Garcia-Domingos, J. Juan-Alcañiz, J. Gascon and F. Kapteijn, *Appl. Catal. A-Gen.*, 2011, **391**, 261-267.
21. H. Thakkar, S. Eastman, Q. Al-Naddaf, A. A. Rownaghi and F. Rezaei, *ACS Appl. Mater. Inter.*, 2017, **9**, 35908-35916.
22. T. Tian, Z. Zeng, D. Vulpe, M. E. Casco, G. Divitini, P. A. Midgley, J. Silvestre-Albero, J. C. Tan, P. Z. Moghadam and D. Fairen-Jimenez, *Nat. Mater.*, 2018, **17**, 174-179.
23. W. Y. Hong, S. P. Perera and A. D. Burrows, *Microporous Mesoporous Mater.*, 2015, **214**, 149-155.
24. Q. Fu, L. Wen, L. Zhang, X. Chen, D. Pun, A. Ahmed, Y. Yang and H. Zhang, *ACS Appl. Mater. Inter.*, 2017, **9**, 33979-33988.

25. Y. Zhang, X. Feng, S. Yuan, J. Zhou and B. Wang, *Inorg. Chem. Front.*, 2016, **3**, 896-909.
26. Y.-H. Shih, K.-Y. Wang, B. Singco, C.-H. Lin and H.-Y. Huang, *Langmuir*, 2016, **32**, 11465-11473.
27. Y. Chen, X. Huang, S. Zhang, S. Li, S. Cao, X. Pei, J. Zhou, X. Feng and B. Wang, *J. Am. Chem. Soc.*, 2016, **138**, 10810-10813.
28. M. N. Channell, M. Sefa, J. A. Fedchak, J. Scherschligt, M. Bible, B. Natarajan, N. N. Klimov, A. E. Miller, Z. Ahmed and M. R. Hartings, *Polym. Adv. Technol.*, 2018, **29**, 867-873.
29. A. Garai, W. Shepherd, J. Huo and D. Bradshaw, *J. Mater. Chem. B*, 2013, **1**, 3678-3684.
30. M. S. Silverstein, *Prog. Polym. Sci.*, 2014, **39**, 199-234.
31. M. G. Schwab, I. Senkovska, M. Rose, M. Koch, J. Pahnke, G. Jonschker and S. Kaskel, *Adv. Eng. Mater.*, 2008, **10**, 1151-1155.
32. L. D. O'Neill, H. Zhang and D. Bradshaw, *J. Mater. Chem.*, 2010, **20**, 5720-5726.
33. M. Mazaj, N. Z. Logar, E. Žagar and S. Kovačič, *J. Mater. Chem. A*, 2017, **5**, 1967-1971.
34. C. L. Calvez, M. Zouboulaki, C. Petit, L. Peeva and N. Shirshova, *RSC Adv.*, 2016, **6**, 17314-17317.
35. Y. Hu, H. Gao, Z. Du, Y. Liu, Y. Yang and C. Wang, *J. Mater. Chem. B*, 2015, **3**, 3848-3857.
36. S. Ungureanu, M. Birot, G. Laurent, H. Deleuze, O. Babot, B. Julián-López, M.-F. Achard, M. I. Popa, C. Sanchez and R. Backov, *Chem. Mater.*, 2007, **19**, 5786-5796.
37. X. Li, G. Sun, Y. Li, J. C. Yu, J. Wu, G. H. Ma and T. Ngai, *Langmuir*, 2014, **30**, 2676-2683.
38. I. Gurevitch and M. S. Silverstein, *J. Polym. Sci., Part A: Polym. Chem.*, 2010, **48**, 1516-1525.
39. Y. F. Yang, F. W. Wang,Q. H. Yang, H. R. Liu, H. L. Jiang and H. X. Xu, *ACS Appl. Mater. Inter.*, 2014, **6**, 18163-18171.
40. J. Yin, T. Q. Zhang, E. Schulman, D. X. Liu and J. Q. Meng, *J. Mater. Chem. A.*, 2018, 6, 8441-8448.
41. J. Huo, M. Marcello, A. Garai and D. Bradshaw, *Adv. Mater.*, 2013, **25**, 2717-2722.
42. B. Xiao, Q. Yuan and R. A. Williams, *Chem. Commun.*, 2013, **49**, 8208-8210.
43. X.-C. Huang, Y.-Y. Lin, J.-P. Zhang and X.-M. Chen, *Angew. Chem. Int. Ed.*, 2006, **45**, 1557-1559.
44. K. S. Park, Z. Ni, A. P. Cote, J. Y. Choi, R. D. Huang, F. J. Uribe-Romo, H. K. Chae, M. O'Keeffe and O. M. Yaghi, *Proc. Natl. Acad. Sci. U. S. A.*, 2006, **103**, 10186-10191.
45. Y. Chevalier and M.-A. Bolzinger, *Colloids Surf. Physicochem. Eng. Aspects*, 2013, **439**, 23-34.
46. H. Duan, D. Wang, N. S. Sobal, M. Giersig, D. G. Kurth and H. Möhwald, *Nano Lett.*, 2005, **5**, 949-952.
47. M. E. Leunissen, A. Van Blaaderen, A. D. Hollingsworth, M. T. Sullivan and P. M. Chaikin, *Proc. Natl. Acad. Sci. U. S. A.*, 2007, **104**, 2585-2590.
48. Y. Lin, H. Skaff, T. Emrick, A. D. Dinsmore and T. P. Russell, *Science*, 2003, **299**, 226-229.
49. S. R. Venna, J. B. Jasinski and M. A. Carreon, *J. Am. Chem. Soc.*, 2010, **132**, 18030-18033.
50. T. T. Y. Tan, J. T. M. Cham, M. R. Reithofer, T. S. A. Hor and J. M. Chin, *Chem. Commun.*, 2014, **50**, 15175-15178.
51. V. O. Ikem, A. Menner, T. S. Horozov and A. Bismarck, *Adv. Mater.*, 2010, **22**, 3588-3592.
52. Q. Q. Liu, L. Wang, A. G. Xiao, H. J. Yu, Q. H. Tan, J. H. Ding and G. Q. Ren, *J. Phys. Chem. C*, 2008, **112**, 13171-13174.
53. W.-Q. Zhou, T.-Y. Gu, Z.-G. Su and G.-H. Ma, *Polymer*, 2007, **48**, 1981-1988.
54. K. Y. Tan, J. E. Gautrot and W. T. S. Huck, *Langmuir*, 2011, **27**, 1251-1259.
55. B. Valizadeh, T. N. Nguyen, B. Smit and K. C. Stylianou, *Adv. Funct. Mater.*, 2018, **28**, 1801596.
56. P. J. Colver and S. A. F. Bon, *Chem. Mater.*, 2007, **19**, 1537-1539.
57. V. C. Dewoolkar, L. N. Jeong, D. W. Cook, K. M. Ashraf, S. C. Rutan and M. M. Collinson, *Anal. Chem.*, 2016, **88**, 5941-5949.
58. H. Y. Zhang, J. J. Ou, Z. S. Liu, H. W. Wang, Y. M. Wei and H. F. Zou, *Anal. Chem.*, 2015, **87**, 8789-8797.
59. A. Maniquet, N. Bruyer, G. Raffin, F. Baco-Antionali, C. Demesmay, V. Dugas and J. Randon, *J. Chromatogr. A*, 2017, **1504**, 105-111.
60. V. O. Ikem, A. Menner and A. Bismarck, *Soft Matter.*, 2011, **7**, 6571-6577.
61. J. H. Cavka, S. Jakobsen, U. Olsbye, N. Guillou, C. Lamberti, S. Bordiga and K. P. Lillerud, *J. Am. Chem. Soc.*, 2008, **130**, 13850-13851.
62. G. Ferey, C. Mellot-Draznieks, C. Serre, F. Millange, J. Dutour, S. Surble and I. Margiolaki, *Science*, 2005, **309**, 2040-2042.
63. S. S.-Y. Chui, S. M.-F. Lo, J. P. H. Charmant, A. G. Orpen and I. D. Williams, *Science*, 1999, **283**, 1148-1150.
64. G. Majano, O. Martin, M. Hammes, S. Smeets, C. Baerlocher and J. Pérez-Ramírez, *Adv. Funct. Mater.*, 2014, **24**, 3855-3865.
65. C. V. McGuire and R. S. Forgan, *Chem. Commun.*, 2015, **51**, 5199-5217.
66. L. Chen, X. Ding, J. Huo, S. El Hankari and D. Bradshaw, *J. Mater. Sci.*, 2018, DOI: 10.1007/s10853-018-2835-x.
67. G. Li, Q. Liu, B. Xia, J. Huang, S. Li, Y. Guan, H. Zhou, B. Liao, Z. Zhou and B. Liu, *Eur. Polym. J.,* 2017, **91**, 242–247.
68. F. Yi, F. Xu, Y. Gao, H. Li and D. Chen, *RSC Adv.*, 2015, **5**, 40227-40235.
69. U. P. N. Tran, K. K. A. Le and N. T. S. Phan, *Acs Catal.*, 2011, **1**, 120-127.
70. R. Narayanan and M. A. El-Sayed, *J. Am. Chem. Soc.*, 2003, **125**, 8340-8347.
71. H. M. Torres Galvis, J. H. Bitter, C. B. Khare, M. Ruitenbeek, A. I. Dugulan and K. P. de Jong, *Science*, 2012, **335**, 835-838.